Inorganic Chemistry
Article

Inorg. Chem. **2010**, *49*, 4073–4083 **4073**
DOI: 10.1021/ic902171j

Excited States of Ru(II) and Re(I) Bipyridyl Complexes Attached to Cyclotriphosphazenes: A Synthetic, Spectroscopic, and Computational Study

Raphael Horvath,[†] Carl A. Otter,[‡] Keith C. Gordon,*[,†] Andrew M. Brodie,*[,‡] and Eric W. Ainscough*[,‡]

[†]*MacDiarmid Institute for Advanced Materials and Nanotechnology, Department of Chemistry, University of Otago, Dunedin, New Zealand, and* [‡]*Chemistry-Institute of Fundamental Sciences, Massey University, Palmerston North, New Zealand*

Received November 3, 2009

A series of new cyclotriphosphazene ligands substituted with pendant 2,2′-bipyridyl moieties, namely, bis[(1,1′-biphenyl)-2,2′-dioxy](2,2′-bipyridyl-3,3′-dioxy)cyclotriphosphazene (L^1), bis[(1,1′-biphenyl)-2,2′-dioxy][bis{4-(2,2′-bipyridin)-4-yl-phenyoxy}]-cyclotriphosphazene (L^2), (pentaphenoxy)[4-(2,2′-bipyridin)-4-yl-phenyoxy]cyclotriphosphazene (L^3), and (pentaphenoxy) [4-{6-phenyl(2,2′-bipyridin)-4-yl}-phenoxy]cyclotriphosphazene (L^4), has been used to synthesize the ruthenium(II) and rhenium(I) complexes, $[(L)Ru(bpy)_2](PF_6)_4$ (L = L^1 or L^3), $[(L^2)\{Ru(bpy)_2\}_2](PF_6)_4$, $[(L)Re(CO)_3Cl]$ (L = L^1, L^3 or L^4), and $[(L^2)\{Re(CO)_3Cl\}_2]$. Single crystal X-ray structures of $[(L^1)Re(CO)_3Cl]$ and $[(L^4)Re(CO)_3Cl]$ show the bipyridyl component of the cyclotriphosphazene substituted ligands is bound to the Re(I) giving a distorted octahedral "N_2C_3Cl" coordination sphere in both cases. Density functional theory (DFT) methods were employed to model the ground-state vibrational properties of the molecules, and their accuracies verified using vibrational spectroscopy. Electronic transitions were identified using UV−visible and resonance Raman spectroscopic techniques, aided by time-dependent (TD) DFT methods. Transient resonance Raman spectra of the excited states of the compounds were acquired and found to be comparable to those reported for studied metal bipyridyl units lacking the cyclotriphosphazene substituents. The cyclotriphosphazene unit has little effect on the properties of the metal bipyridyl chromophore.

Introduction

Complexes of heavy transition metals such as rhenium and ruthenium are suitable for use as dyes in Gratzel cells as well as emitting centers in organic light emitting diodes (OLEDs).[1−4] As such devices become commercialized, improved materials technologies and production methods become more important. OLEDs have great potential in display technology; however, currently they suffer from limited lifetimes and are thus largely unsuitable for commercial use. It has been determined that both emissive and charge-transporting layers and their communication can have an effect on the degradation rate.[5] For example the rates of diffusion of radicals as well as the stability of the host material are important. It is therefore advantageous to utilize materials in the construction of OLEDs where parameters such as the glass transition temperature (T_g) and stability against various influences can be carefully controlled. Polymeric and cyclic phosphazenes (Chart 1) are classes of compounds where such control is possible. A wide range of substituents can be attached to the phosphazene scaffold, allowing many possibilities for derivatization. For example, we have recently explored the reactions of cyclic phosphazenes substituted with pyridine, phenanthroline, and phosphine ligand moieties and found them to have a rich metal-ion coordination chemistry.[6−12] There are also many other examples of metal containing cyclic phosphazene compounds in which pyrazolyl, nitrile, or ferrocenyl ligands, to name a few, have been incorporated.[13,14] The

*To whom correspondence should be addressed. E-mail: kgordon@chemistry.otago.ac.nz (K.C.G.), a.brodie@massey.ac.nz (A.M.B.), e.ainscough@massey.ac.nz (E.W.A.).

(1) O'Regan, B.; Graetzel, M. *Nature* **1991**, *353*, 737–740.
(2) Tang, C. W.; VanSlyke, S. A. *Appl. Phys. Lett.* **1987**, *51*, 913–915.
(3) Lundin, N. J.; Blackman, A. G.; Gordon, K. C.; Officer, D. L. *Angew. Chem., Int. Ed.* **2006**, *45*, 2582–2584.
(4) Welter, S.; Brunner, K.; Hofstraat, J. W.; DeCola, L. *Nature* **2003**, *421*, 54–57.
(5) Kondakov, D. Y.; Lenhart, W. C.; Nichols, W. F. *J. Appl. Phys.* **2007**, *101*, 024512/1–024512/7.
(6) Ainscough, E. W.; Brodie, A. M.; Depree, C. V.; Moubaraki, B.; Murray, K. S.; Otter, C. A. *Dalton Trans.* **2005**, 3337–3343.
(7) Ainscough, E. W.; Brodie, A. M.; Depree, C. V.; Jameson, G. B.; Otter, C. A. *Inorg. Chem.* **2005**, *44*, 7325–7327.
(8) Ainscough, E. W.; Brodie, A. M.; Chaplin, A. B.; O'Connor, J. M.; Otter, C. A. *Dalton Trans.* **2006**, 1264–1266.
(9) Ainscough, E. W.; Brodie, A. M.; Jameson, G. B.; Otter, C. A. *Polyhedron* **2007**, *26*, 460–471.
(10) Ainscough, E. W.; Brodie, A. M.; Derwahl, A.; Kirk, S.; Otter, C. A. *Inorg. Chem.* **2007**, *46*, 9841–9852.
(11) Ainscough, E. W.; Brodie, A. M.; Davidson, R. J.; Otter, C. A. *Inorg. Chem. Commun.* **2008**, *11*, 171–174.
(12) Ainscough, E. W.; Brodie, A. M.; Davidson, R. J.; Moubaraki, B.; Murray, K. S.; Otter, C. A.; Waterland, M. R. *Inorg. Chem.* **2008**, *47*, 9182–9192.
(13) Chandrasekhar, V.; Thilagar, P.; Murugesa Pandian, B. *Coord. Chem. Rev.* **2007**, *251*, 1045–1074.
(14) Pertici, P.; Vitulli, G.; Gleria, M.; Facchin, G.; Milani, R.; Bertani, R. *Macromol. Symp.* **2006**, *235*, 98–114.

© 2010 American Chemical Society
Published on Web 04/08/2010

Chart 1. Generic Polyphosphazene and Cyclotriphosphazene (CTP) Structures

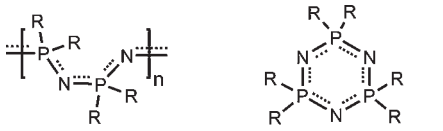

Polyphosphazene Cyclotriphosphazene

binding of metal ions that have valuable photophysical properties, such as ruthenium and rhenium, have been reported in some of these systems.[13] A recent report details the preparation of an OLED device that incorporates an iridium complex bonded to a cyclotriphosphazene dendrimer.[15] In some cases the chemistry has also been extended to the polyphosphazene analogues, yielding the metal-rich macromolecular species. Since the flexibility of the polymer backbone can be controlled by the choice of the substituents incorporated, properties such as T_g can also be controlled.[16] Hence, the polymeric and cyclic phosphazene systems are promising candidates to explore as hosts for dyes in OLED or photochemical energy cell systems. To allow the efficient design of devices it is advantageous to know in detail the effect of phosphazene attachment on fluorophore behavior.

This study examines the properties of transition-metal fluorophores attached to cyclotriphosphazene (CTP) in comparison to the free fluorophores with reference to their photophysical properties. It has been carried out using a variety of ground and excited state spectroscopic techniques including FT-Raman, resonance Raman, and transient resonance Raman (TR^2) and has been supplemented by density functional theory (DFT) calculations to obtain a theoretical insight. The compounds studied here are derivatives of the well-known ruthenium *tris*-(bipyridyl)ruthenium(II) cation, $[Ru(bpy)_3]^{2+}$, and bipyridyltricarbonylchlororhenium(I), $[Re(bpy)(CO)_3Cl]$, fluorophores. This is the first time cyclic phosphazene systems containing these species have been reported. It is interesting to determine if the attachment of metal units to the CTP function dramatically alters the emissive properties imbued by the metal complex or does the CTP unit act as an electronically mute scaffold?

Experimental Section

General Procedures. Analytical grade solvents were used without further purification with the exception of tetrahydrofuran (THF) which was distilled from sodium/benzophenone. $[Re(CO)_5Cl]$ was obtained from Pressure Chemicals (Pittsburgh) and tetrabutylammonium bromide (TBAB) was obtained from Merck. $[N_3P_3(biph)_2Cl_2]$ (biph = 2,2′-oxybiphenyl),[17] $[N_3P_3(OPh)_2Cl]$ (OPh = oxyphenyl),[18] 3,3′-dihydroxybipyridine [$(HO)_2$bpy],[19] 4-(4-hydroxyphenyl)-2,2′-bipyridine (HOPhbpy),[20] 4-(4-hydroxyphenyl)-6-phenyl-2,2′-bipyridine[21] (HOPhbpyPh), and $[Ru(bpy)_2Cl_2]2H_2O$[22] were prepared according to literature procedures.

Synthesis. **$[N_3P_3(biph)_2(O_2bpy)]$ (L^1).** A mixture of $[N_3P_3(biph)_2Cl_2]$ (0.391 g, 0.68 mmol), Cs_2CO_3 (1 g, 3.07 mmol), and $(HO)_2$bpy (0.128 g, 0.68 mmol) in acetone (30 mL) was heated at reflux over 5 h. The mixture was taken to dryness, and the residue was extracted with CH_2Cl_2. The extract was filtered through Celite and taken to dryness on a rotary evaporator. Chromatography of the residue on silica using CH_2Cl_2/MeOH (98:2) as eluent gave the product as a white solid (0.320 g) which was recrystallized from CH_2Cl_2/hexane. Yield: 0.280 g (60%). Anal. Required for $C_{34}H_{22}N_5O_6P_3$: C, 59.23; H, 3.22; N, 10.16%. Found: C, 58.70; H, 3.32; N, 10.20%. ESMS: *m*/*z* 690 $[M+H]^+$. $^{31}P\{^1H\}$ NMR ($CDCl_3$): δ 24.9−27.5 (m, 3P) ^1H NMR ($CDCl_3$): δ 8.72 (br m, 2H), 7.71 (m, 2H), 7.51 (m, 4H), 7.48−7.38 (m, 6H), 7.37−7.28 (m, 8H).

$[N_3P_3(biph)_2(OPhbpy)_2]\cdot 0.25CH_2Cl_2$ (L^2). To a solution of HOPhbpy (0.40 g, 1.6 mmol) in THF (30 mL) was added NaH (0.65 g of a 60% dispersion in oil, 1.6 mmol NaH). The solution was stirred at room temperature over 3 h, and TBAB (0.03 g) and $[N_3P_3(biph)_2Cl_2]$ (0.462 g, 0.8 mmol) were added. The mixture was heated at reflux over 15 h, allowed to cool, and the THF removed on a rotary evaporator. The crude residue was extracted with CH_2Cl_2 and filtered through Celite. The CH_2Cl_2 extract was taken to dryness, and the residue purified by column chromatography on silica using MeOH (0−4%) in CH_2Cl_2 as eluent. Recrystallization from CH_2Cl_2/hexane and drying at 70 °C under vacuum afforded the product as a white solid. Yield: 0.700 g (87%). Anal. Required for $C_{56.25}H_{38.5}Cl_{0.5}N_7O_6P_3$: C, 66.23; H, 3.78; N, 9.61%. Found: C, 66.44; H, 3.85; N, 9.83%. ESMS: *m*/*z* 998 $[M+H]^+$. $^{31}P\{^1H\}$ NMR ($CDCl_3$): δ 25.43 (d, 2P, J_{PP} = 93 Hz, phosphazene), 9.67 (t, P, J_{PP} = 95 Hz, phosphazene). ^1H NMR ($CDCl_3$): δ 9.25 (s, 2H), 9.10 (d, 2H), 8.89 (m, 4H), 8.24 (m, 2H), 8.03 (m, 4H), 7.94 (m, 2H), 7.69 (m, 2H), 7.59 (m, 4H), 7.50 (m, 4H), 7.40 (m, 4H), 7.31 (m, 4H), 7.15 (m, 4H).

$[N_3P_3(OPh)_5(OPhbpy)]$ (L^3). To a solution of HOPhbpy (0.145 g, 0.60 mmol) in THF (30 mL) was added NaH (0.024 g of a 60% dispersion in oil, 0.60 mmol NaH), and the mixture was stirred over 0.5 h. $[N_3P_3(OPh)_5Cl]$ (0.373 g, 0.60 mmol) and TBAB (0.050 g, 0.16 mmol) were added, and the mixture was heated at reflux overnight. The THF was removed on a rotary evaporator, and the residue was extracted into CH_2Cl_2. The organic extract was filtered through Celite and taken to dryness on a rotary evaporator. Chromatography of the residue on silica using CH_2Cl_2/MeOH (98:2) as eluent afforded the product as an oil which was dried under vacuum at 50 °C to give a waxy solid. Yield: 0.350 g (70%). Anal. Required for $C_{46}H_{36}N_5O_6P_3$: C, 65.17; H, 4.28; N, 8.26%. Found: C, 65.04; H, 4.47; N, 8.29%. ESMS: *m*/*z* 848 $[M+H]^+$. $^{31}P\{^1H\}$ NMR ($CDCl_3$): δ 10.9−9.2 (m, 3P). ^1H NMR ($CDCl_3$): δ 8.74 (m, 2H), 8.68 (br s, H), 8.55 (m, H), 7.89 (m, H), 7.55 (m, 2H), 7.50 (m, H), 7.37 (m, H), 7.21−7.06 (m, 15H), 7.03 (m, 2H), 6.99−6.86 (m, 10H).

$[N_3P_3(OPh)_5(OPhbpyPh)]$ (L^4). A mixture of HOPhbpyPh (0.163 g, 0.5 mmol) and NaH (0.020 g of a 60% dispersion in oil, 0.5 mmol NaH) in THF (35 mL) was allowed to stir at room temperature over 1 h. $[N_3P_3(OPh)_5Cl]$ (318 mg, 0.5 mmol) and TBAB (20 mg) were added, and the mixture was heated at reflux overnight. The THF was removed on a rotary evaporator, the residue extracted with CH_2Cl_2, and the extract filtered through Celite. Chromatography on silica using MeOH (0−2%) in CH_2Cl_2 as eluent yielded the product as a clear oil, which was dried under vacuum. Yield: 0.401 g (87%). Anal. Required for $C_{51}H_{40}N_6O_6P_3$: C, 67.61; H, 4.36; N, 7.58%. Found: C, 67.74; H, 4.57; N, 7.56%. ESMS: *m*/*z* = 924 $[M+H]^+$. $^{31}P\{^1H\}$ NMR ($CDCl_3$): δ 9.71−7.98 (m, 3P). ^1H NMR ($CDCl_3$): δ 8.71 (m, H), 8.67 (m, H), 8.57 (s, H), 8.18 (m, 2H), 7.88−7.83 (m, 2H), 7.60−7.49 (m, 4H), 7.45 (m, H), 7.33 (m, H) 7.20−7.06 (m, 15H), 7.03 (m, 2H), 6.99−6.88 (m, 10H).

$[(L^1)Ru(bpy)_2](PF_6)_2\cdot 0.5CH_2Cl_2$ (1). A mixture of L^1 (0.050 g, 0.073 mmol) and $[Ru(bpy)_2Cl_2]\cdot 2H_2O$ (0.038 g, 0.073 mmol) in MeOH (30 mL) was heated at reflux overnight. The red

(15) Bolink, H. J.; Santamaria, S. G.; Sudhakar, S.; Zhen, C.; Sellinger, A. *Chem. Commun.* **2008**, 618–620.
(16) Allcock, H. R. *Chemistry and Applications of Polyphosphazenes*; Wiley: New York, 2003; p 774.
(17) Carriedo, G. A.; Fernandez-Catuxo, L.; Alonso, F. J. G.; Gomez-Elipe, P.; Gonzalez, P. A. *Macromolecules* **1996**, *29*, 5320–5325.
(18) Allcock, H. R.; Laredo, W. R.; deDenus, C. R.; Taylor, J. P. *Macromolecules* **1999**, *32*, 7719–7725.
(19) Tiecco, M.; Testaferri, L.; Tingoli, M.; Chianelli, D.; Montanucci, M. *Synthesis* **1984**, 736–738.
(20) Hayes, M. A.; Meckel, C.; Schatz, E.; Ward, M. D. *J. Chem. Soc., Dalton Trans.* **1992**, 703–708.
(21) Neve, F.; Ghedini, M.; Francescangeli, O.; Campagna, S. *Liq. Cryst.* **1998**, *24*, 673–680.
(22) Godwin, J. B.; Meyer, T. J. *Inorg. Chem.* **1971**, *10*, 2150–2153.

solution was allowed to cool and filtered through Celite. A solution of NH_4PF_6 in MeOH was added to the filtrate to produce a red precipitate that was collected by filtration and washed with Et_2O. The product was purified by chromatography on alumina using MeCN as eluent and recrystallized from CH_2Cl_2/hexane. Yield: 0.050 g (48%). Anal. Required for $C_{54.5}H_{39}ClF_{12}N_9O_6P_5Ru$: C, 45.60; H, 2.72; N, 8.78%. Found: C, 45.33; H, 2.92; N, 8.62%. ESMS: m/z 1248 $[M+PF_6]^+$, 522 $[M]^{2+}$. ^1H NMR (d^6−DMSO): δ 8.79 (m, 4H), 8.29 (m, 2H), 8.13 (m, 4H), 7.89 (m, 2H), 7.33−7.62 (m, 8H), 7.60 (m, 2H), 7.57−7.41 (m, 12H), 7.37 (m, 2H), 7.30 (m, 2H). $^{31}P\{^1H\}$ NMR (d^6−DMSO): δ 24.9−24.3 (m, 2P), 22.0−20.8 (m, P), −144.0 (sept, 2P, J_{PF} = 729 Hz).

[(L^3)Ru(bpy)$_2$](PF$_6$)$_2$ (2). A mixture of L^3 (0.204 g, 0.24 mmol) and $[Ru(bpy)_2Cl_2]\cdot 2H_2O$ (0.125 g, 0.24 mol) was heated at reflux in MeOH (25 mL) over 24 h. A solution of NH_4PF_6 in MeOH was added to produce an orange precipitate which was collected by filtration and washed with Et_2O. Yield: 0.250 g (67%). Anal. Required for $C_{66}H_{52}F_{12}N_9O_6P_5Ru$: C, 51.11; H, 3.38; N, 8.13%. Found: C, 50.56; H, 3.54; N, 8.04%. ESMS: m/z 1058 $[M+2PF_6]^{2+}$, 657 $[M+PF_6]^{3+}$, 457 $[M]^{4+}$. ^1H NMR (d^6−DMSO): δ 9.08 (m, 2H), 8.83 (m, 4H), 8.16 (m, 5H), 7.93 (m, 2H), 7.81 (m, 2H), 7.72 (m, 5H), 7.51 (m, 5H), 7.29−7.15 (m, 13H), 7.15−7.03 (m, 4H), 6.91 (m, 4H), 6.81 (m, 6H). $^{31}P\{^1H\}$ NMR (d^6−DMSO): δ 9.0 (m, 3P), −144.1 (sept, 2P, J_{PF} = 709 Hz).

[(L^2){Ru(bpy)$_2$}$_2$](PF$_6$)$_4\cdot$CH$_2$Cl$_2$ (3). A mixture of L^2 (0.100 g, 0.100 mmol) and $[Ru(bpy)_2Cl_2]\cdot 2H_2O$ (0.104 g, 0.200 mmol) was heated at reflux in MeOH (25 mL) over 24 h. A solution of NH_4PF_6 in MeOH was added to produce an orange precipitate which was collected by filtration and washed with Et_2O. The precipitate was dissolved in CH_2Cl_2 and hexane was added, producing a red oil that formed a glassy solid upon standing in a freezer. Yield: 0.160 g (64%). Anal. Required for $C_{97}H_{72}Cl_2F_{24}N_{15}O_6P_7Ru_2$: C, 46.80; H, 2.92; N, 8.44%. Found: C, 46.78; H, 2.81; N, 8.48%. ESMS: m/z 1406 $[M+PF_6]^+$, 630 $[M]^{2+}$. ^1H NMR (d^6−DMSO): δ 9.14 (s, 2H), 9.08 (m, 2H), 8.82 (m, 8H), 8.26−8.09 (m, 14H), 7.89 (m, 2H), 7.79 (m, 2H), 7.75−7.62 (m, 14H), 7.56 (m, 4H), 7.53−7.45 (m, 14H), 7.42 (m, 4H), 7.15 (m, 4H). $^{31}P\{^1H\}$ NMR (d^6−DMSO): δ 25.3 (d, 2P, J_{PP} = 92 Hz), 9.86 (m, P), −144.1 (sept, 4P, J_{PF} = 732 Hz).

[(L^1)Re(CO)$_3$Cl]$\cdot$0.5C$_7$H$_8$ (4). A mixture of L^1 (0.050 g, 0.073 mmol) and $[Re(CO)_5Cl]$ (0.026 g, 0.072 mmol) was heated at reflux in toluene (25 mL) over 5 h. The yellow solution was concentrated on a rotary evaporator to approximately 5 mL and the yellow precipitate that formed was collected by filtration, washed with Et_2O, and dried under vacuum at 40 °C. Yield: 0.057 g (76%). Anal. Required for $C_{40.5}H_{26}ClN_5O_9P_3Re$: C, 46.67; H, 2.64; N, 6.72%. Found: C, 46.94; H, 2.54; N, 6.81%. $^{31}P\{^1H\}$ NMR ($CDCl_3$): δ 9.13 (m, 3P). ^1H NMR ($CDCl_3$): δ 8.98 (m, 2H), 7.98 (m, 2H), 7.67 (m, 2H), 7.57 (m, 4H), 7.47 (m, 4H), 7.41−7.34 (m, 8H).

[(L^3)Re(CO)$_3$Cl] (5). A mixture of L^3 (0.050 g, 0.059 mmol) and $[Re(CO)_5Cl]$ (0.018 g, 0.049 mmol) in toluene (10 mL) was heated at reflux over 5 h and stirred at room temperature overnight. The orange solution was filtered, taken to dryness on a rotary evaporator, and the residue was dissolved in CH_2Cl_2 (ca. 10 mL). Hexane was added to this solution, and the volume was reduced to produce a yellow precipitate that was collected by filtration and dried under vacuum at 40 °C. Yield 0.040 g (59%). Anal. Required for $C_{49}H_{36}ClN_5O_9P_3Re$: C, 51.02; H, 3.15; N, 6.07%. Found: C, 51.17; H, 3.19; N, 6.11%. $^{31}P\{^1H\}$ NMR ($CDCl_3$): δ 9.55−8.97 (m, 3P). ^1H NMR ($CDCl_3$): δ 9.11 (m, H), 9.06 (m, H), 8.27 (m, H), 8.21 (s, H), 8.09 (m, H), 7.59 (m, 2H), 7.50 (m, 2H), 7.25−7.10 (m, 17H), 7.04 (m, 4H), 6.98−6.86 (m, 6H).

[(L^2){Re(CO)$_3$Cl}$_2$]$\cdot$CH$_2$Cl$_2$ (6). A mixture of L^2 (0.100 g, 0.100 mmol) and $[Re(CO)_5Cl]$ (0.072 g, 0.199 mmol) in toluene (15 mL) was heated at reflux over 3 h then stirred at room temperature overnight. A yellow precipitate formed that was collected by filtration and washed with Et_2O. The precipitate was a mixture of singly and doubly substituted material (approximately 1:10). The precipitate was dissolved in a solution of CH_2Cl_2 (20 mL) and $CHCl_3$(10 mL) which was allowed to evaporate slowly over 2 weeks. Two microcrystalline crops of clean doubly substituted material were collected during this time. Yield: 0.075 g (44%). Anal. Required for $C_{63}H_{40}Cl_4N_7O_{12}P_3Re_2$: C, 44.66; H, 2.38; N, 5.79%. Found: C, 44.55; H, 2.31; N, 5.85%. $^{31}P\{^1H\}$ NMR (d^6−DMSO): δ 25.07 (d, 2P, J_{PP} = 92 Hz), δ 10.01 (t, P, J_{PP} = 92 Hz). ^1H NMR (d^6−DMSO): δ 9.09 (s, 2H), 9.07−9.02 (m, 6H), 8.38 (m, 2H), 8.32 (m, 4H), 8.13 (m, 2H), 7.80 (m, 2H), 7.70 (m, 4H), 7.64 (m, 4H), 7.54 (m, 4H), 7.46 (m, 4H), 7.23 (m, 4H).

[(L^4)Re(CO)$_3$Cl] (7). A suspension of L^4 (0.050 g, 0.054 mmol) and $[Re(CO)_5Cl]$ (0.194 g, 0.054 mmol) in toluene (10 mL) was heated at reflux over 5 h. The resulting orange solution was filtered, and the toluene removed on a rotary evaporator. The residue was dissolved in CH_2Cl_2 (ca. 3 mL) and filtered through a plug of Celite. Hexane was added to the filtrate, and a crop of crystalline material developed over 48 h. A crystal suitable for X-ray diffraction data collection was selected, and the bulk was collected by filtration and dried under vacuum. Yield: 0.045 g (68%). Anal. Required for $C_{55}H_{40}ClN_5O_9P_3Re$: C, 53.73; H, 3.28; N, 5.70%. Found: C, 53.76; H, 3.38; N, 5.63%. ^1H NMR ($CDCl_3$): δ 9.14 (m, H), 8.31 (m, H), 8.25 (m, H), 8.09 (m, H), 7.76−7.64 (m, 3H), 7.64−7.58 (m, 3H), 7.56−7.48 (m, 3H), 7.25−7.07 (m, 17H), 7.07−7.01 (m, 4H), 6.97−6.85 (m, 6H). $^{31}P\{^1H\}$ NMR ($CDCl_3$): δ 9.6−9.0 (m, 3P).

Crystallography. Vapor diffusion of pentane into a $CDCl_3$ solution of **4** afforded yellow blocks of $\mathbf{4}\cdot 3CDCl_3$, and yellow plates of $\mathbf{7}\cdot 0.26H_2O$ were grown from CH_2Cl_2/hexane solution. The X-ray data were collected on a Siemens P4 four circle diffractometer, using a Siemens SMART 1K CCD area detector. The crystals were mounted in an inert oil and irradiated with graphite-monochromated Mo−Kα (λ = 0.71073 Å) X-rays. The data were collected by the SMART program and processed with SAINT to apply Lorentz and polarization corrections to the diffraction spots (integrated 3 dimensionally). Crystal data are given in Table 1. The structures were solved by direct methods and refined using the SHELXTL program.[23] Hydrogen atoms were calculated at ideal positions.

Table 1. Crystal and Refinement Data for Compounds $\mathbf{4}\cdot 3CHCl_3$ and $\mathbf{7}\cdot 0.26H_2O$

	$\mathbf{4}\cdot 3CHCl_3$	$\mathbf{7}\cdot 0.26H_2O$
empirical formula	$C_{40}H_{25}C_{110}N_5O_9P_3Re$	$C_{55}H_{42.52}ClN_5O_{9.26}P_3Re$
M	1353.26	1234.18
T (K)	190(2)	190(2)
crystal system	triclinic	triclinic
space group	$P\bar{1}$	$P\bar{1}$
a (Å)	8.5198(6)	11.6960(6)
b (Å)	14.6205(10)	11.7241(6)
c (Å)	20.7929(14)	21.3092(11)
α (deg)	105.593(2)	76.201(3)
β (deg)	98.725(2)	83.228(3)
γ (deg)	98.796(2)	66.364(3)
V (Å^3)	2414.3(3)	2598.8(2)
Z	2	2
μ (MoKα) (mm^{-1})	3.229	2.545
ρ_{calc} (g cm^{-3})	1.862	1.577
2θ max (deg)	50.7	50.7
no. of unique reflections	8413	9399
data/restraints/parameters	8413/0/613	9399/274/683
final R indices [$I > 2\sigma(I)$]	R_1 = 0.0379, wR_2 = 0.0914	R_1 = 0.0502, wR_2 = 0.1147
R indices (all data)	R_1 = 0.0493, wR_2 = 0.0976	R_1 = 0.0624, wR_2 = 0.1221
goodness of fit on F^2	1.047	1.126

(23) Sheldrick, G. M. *SHELXL Suite of Programs for Crystal Structure Analysis*; Institut für Anorganische Chemie der Universität Göttingen: Göttingen, Germany, 1998.

Instrumentation. Microanalyses were performed by the Campbell Microanalytical Laboratory, University of Otago. ^{1}H NMR spectra were recorded at 162 MHz and ^{31}P{^{1}H} NMR spectra were recorded at 400 MHz on a Bruker Avance 400 spectrometer. Electrospray mass spectra were obtained from CH_3CN solutions on a Micromass ZMD spectrometer run in the positive ion mode. Listed peaks correspond to the most abundant isotopomer; assignments were made by a comparison of observed and simulated spectra. All ground-state vibrational measurements were taken in solid-state KBr disks. FT-IR measurements were obtained using a Perkin-Elmer BX FT-IR spectrometer with Spectrum v2.00 software. The spectra were acquired as 64 co-added scans with a resolution of 4 cm^{-1}. FT-Raman spectra were obtained using a Bruker Equinox 55 interferometer coupled with a FRA-106 Raman module and a D418T liquid-nitrogen-cooled Germanium detector, controlled by the Bruker OPUS v5.5 software package. A Nd:YAG laser operating at 1064 nm and 450 mW was used. The spectra were acquired as 256−2024 co-added scans with a resolution of 4 cm^{-1}. UV−visible absorption spectra of 10^{-4} mol L^{-1} solutions of the compounds were acquired in the range 190−600 nm using a Jasco V-550 spectrophotometer controlled by Spectrum Measurement v1.53.00. Emission spectra were obtained using the setup described by Howell et al.[24,25] In short, the excitation beam from a continuous-wave Innova I-302 krypton-ion laser (Coherent, Inc.) operating at 350.7 nm and collection lens are arranged in a 135° backscattering geometry, which focuses the emission on an Acton Research SpectraPro500i spectrograph. A notch filter is used to remove the laser excitation line. Using a 300 grooves mm^{-1} diffraction grating and four acquisition windows, a wavelength range of 300−950 nm was observed. A similar setup using a 1200 grooves mm^{-1} diffraction grating was used to perform resonance Raman (RR) spectroscopy at excitation wavelengths of 350.7, 406.7, and 413.1 nm.[26,27] Furthermore, a diode-pumped laser (CrystaLaser) at 444.3 nm and a Melles Griot Omnichrome model 543-MAP argon laser at 457.9 and 488.0 nm were used to obtain spectra at these excitation wavelengths. Excited-state transient resonance Raman (TR^2) measurements were performed using 354.7 nm third-harmonic radiation from a Brilliant (Quantel) Nd:YAG pulse laser at power outputs of 0.96, 1.84, and 3.10 mJ/pulse and a repetition rate of 10 Hz. For both RR and TR^2 compounds were in 10^{-3} mol L^{-1} CH_2Cl_2 solutions, which had been degassed using argon for 20 min prior to measurement. The excited state lifetime of argon-purged 10^{-3} mol L^{-1} CH_2Cl_2 solutions was measured using excitation from the Brilliant Nd:YAG laser described above. Emission signals were measured by a Hamamatsu H5783−04 photomultiplier at 580, 620, 660, and 700 nm and read out on a Tektronix TDS 3032B model digital oscilloscope. For each trace the natural logarithm of the emission intensity was plotted against time, and typically these data could be fit linearly with R^2 values greater than 0.95. The errors were estimated using the standard deviation of measurements between each wavelength. No sample degradation was observed for any of the complexes for either TR^2 or emission lifetime measurements.

Computational Details. Density functional theory (DFT) calculations were carried out using the Gaussian 03 Package[28] (Gaussian, Inc.). Frequency and time-dependent (TD) calculations were performed on the optimized ground-state structures. To investigate the triplet state structure of **7**, geometry optimization of the model compound [Re(4,6-dpb)(CO)$_3$Cl] (4,6-dpb = 4,6-diphenyl-2,2′-bipyridine) in a triplet-state configuration were also performed. All calculations employed the B3LYP functional using the 6-31G(d) basis set for the ligands, while heavy metal centers were approximated using LANL2DZ effective core potentials.[29] The output frequencies were scaled by a factor of 0.975[30] and IR and Raman spectra generated using a Lorentzian line-shape with a half-width at half-maximum (HWHM) of 3 cm^{-1}. The vibrational modes and molecular orbitals were visualized using Molden[31] and GaussView v4.1 (Gaussian, Inc.) respectively after extraction from the output files using GaussSum.[32] The accuracy of the calculations was monitored using mean absolute deviation (MAD) values, which are obtained by averaging the absolute difference in cm^{-1} of the 5−10 most prominent experimental peaks to the corresponding calculated peaks in the spectral range 400 cm^{-1} to 1800 cm^{-1}. Carbonyl stretches require different scale-factors[33] and were therefore omitted in the MAD calculations. Unambiguous assignment of vibrational modes from visual comparison of spectra was possible for most peaks. TD-DFT calculations were carried out in a dichloromethane solvent field using the IEF-PCM method,[34,35] which treats the solvent as a continuum containing the solute as a series of interlocking spheres. Geometry optimizations were not carried out in a solvent field, as these are very difficult to achieve for molecules this size; however, correlation is found to be better than for calculations where solvent contributions have been completely neglected.[36,37]

Results and Discussion

Syntheses. The new phosphazene ligands, L^1, L^2, L^3, and L^4, were prepared by the reaction of 1 or 2 equiv of the phenolic bipyridine precursors with $[N_3P_3(biph)_2Cl_2]$ or $[N_3P_3(OPh)_5Cl]$ in the presence of a base (Scheme 1). The reaction of $(HO)_2$bpy with $[N_3P_3(biph)_2Cl_2]$ in acetone using Cs_2CO_3 gives the ligand L^1. The treatment of HOPhbpy with NaH in THF followed by the reaction with $[N_3P_3(biph)_2Cl_2]$ at reflux overnight in the presence of the catalyst TBAB gives the ligand L^2. The reaction of the sodium salt of HOPhbpy or HOPhbpyPh in THF with $[N_3P_3(OPh)_5Cl]$ using TBAB as a catalyst affords the ligands L^3 and L^4. All four ligands were purified by chromatography and L^1 and L^2 were obtained as white solids after recrystallization from CH_2Cl_2/hexane. L^3 and L^4 were obtained as oils after drying under vacuum at 50 °C. Ruthenium *tris*-bipyridyl derivatives of L^1−L^3 were obtained by reacting the ligands with [Ru(bpy)$_2$Cl$_2$] in refluxing MeOH followed by metathesis with NH_4PF_6. The complexes all show characteristic MLCT transitions between 446 and 454 nm and ε per Ru(II) ranges between 11600 and 17300 dm^3 mol^{-1} cm^{-1}. The half wave potentials for the Ru(II)/Ru(III) couple (with respect to the ferrocene/ferrocinium couple) are 0.86 and 0.87 V respectively for $[(L^3)Ru(bpy)_2](PF_6)_2$ and $[(L^2)\{Ru(bpy)_2\}_2](PF_6)_4$ with a value slightly higher for $[(L^1)Ru(bpy)_2](PF_6)_2$ at 0.98 V. The rhenium complexes were prepared from the reaction between [Re(CO)$_5$Cl] and L^1−L^4 in refluxing

(24) Howell, S. L.; Gordon, K. C. *J. Phys. Chem. A* **2004**, *108*, 2536–2544.
(25) Howell, S. L.; Matthewson, B. J.; Polson, M. I. J.; Burrell, A. K.; Gordon, K. C. *Inorg. Chem.* **2004**, *43*, 2876–2887.
(26) Walsh, P. J.; Gordon, K. C.; Lundin, N. J.; Blackman, A. G. *J. Phys. Chem. A* **2005**, *109*, 5933–5942.
(27) Lind, S. J.; Gordon, K. C.; Waterland, M. R. *J. Raman Spectrosc.* **2008**, *39*, 1556–1567.
(28) Frisch, M. J. et al. *Gaussian 03*; Gaussian,Inc.: Wallingford, CT, 2003.
(29) Howell, S. L.; Scott, S. M.; Flood, A. H.; Gordon, K. C. *J. Phys. Chem. A* **2005**, *109*, 3745–3753.
(30) Walsh, P. J.; Gordon, K. C.; Officer, D. L.; Campbell, W. M. *J. Mol. Struc., THEOCHEM* **2006**, *759*, 17–24.
(31) Schaftenaar, G.; Noordik, J. H. *J. Comput.-Aided Mol. Des.* **2000**, *14*, 123–134.
(32) O'Boyle, N. M.; Tenderholt, A. L.; Langner, K. M. *J. Comput. Chem.* **2008**, *29*, 839–845.
(33) Howell, S. L.; Gordon, K. C.; Waterland, M. R.; Leung, K. H.; Phillips, D. L. *J. Phys. Chem. A* **2006**, *110*, 11194–11199.
(34) Chipman, D. M. *J. Chem. Phys.* **2000**, *112*, 5558–5565.
(35) Tomasi, J.; Mennucci, B.; Cances, E. *J. Mol. Struc., THEOCHEM* **1999**, *464*, 211–226.
(36) Charlot, M.-F.; Aukauloo, A. *J. Phys. Chem. A* **2007**, *111*, 11661–11672.
(37) Vlcek, A. J.; Zalis, S. *J. Phys. Chem. A* **2005**, *109*, 2991–2992.

Scheme 1. Synthesis Schemes for the Ligands L^1−L^4 and Numbering for the Ruthenium and Rhenium Complexes

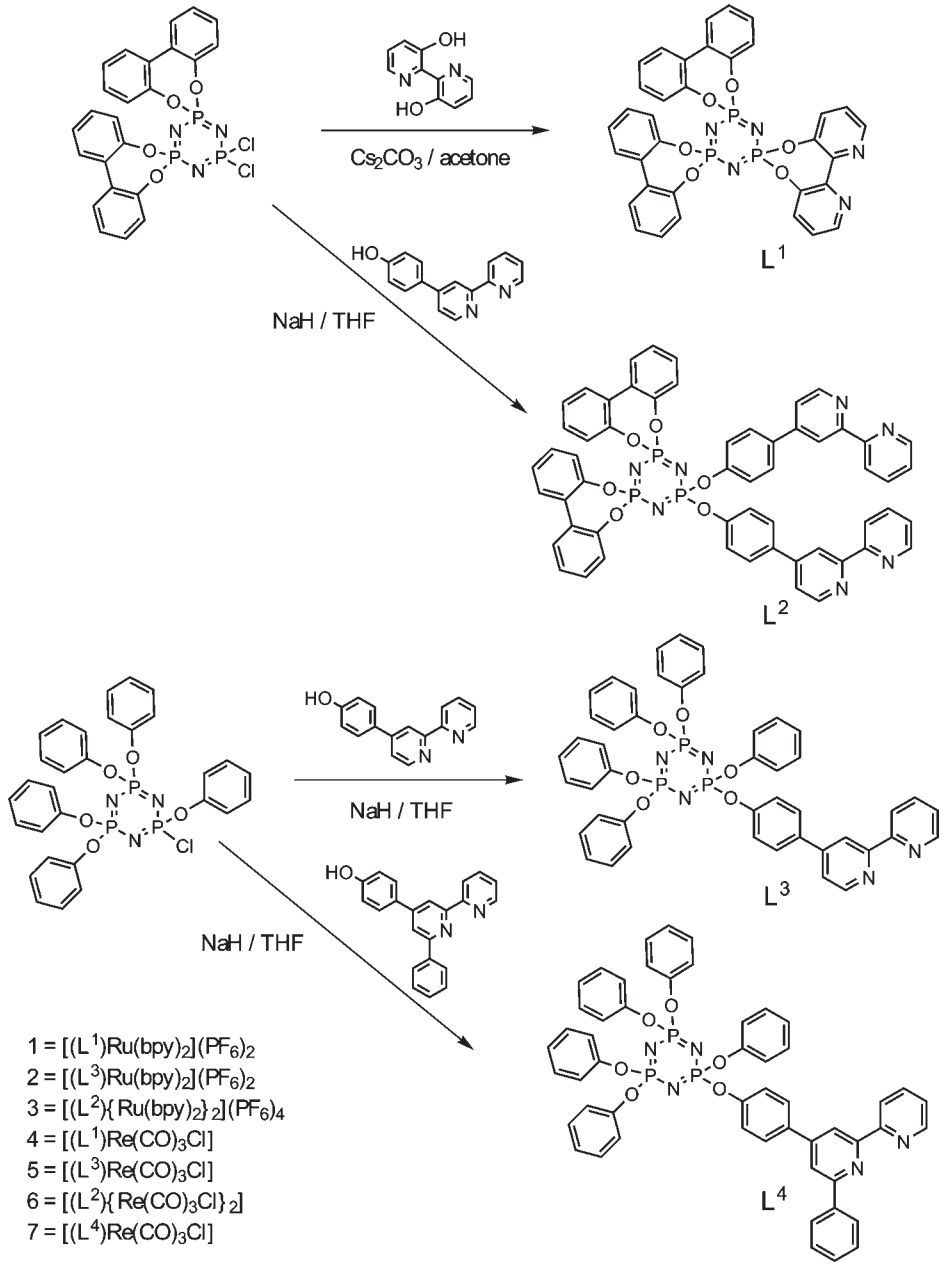

toluene. The materials were purified by recrystallization. Retention of solvent molecules by aromatic phosphazene-based ligands and their complexes is a common occurrence in our experience (even after prolonged drying under vacuum). The presence of solvent is confirmed by the microanalytical data, ^{1}H NMR spectra, and X-ray data where possible. There is a precedent for this behavior in phosphazene chemistry, and it has been exploited in the design of clathrate systems.[38]

X-ray Crystallography. $[(L^1)Re(CO)_3Cl]\cdot 3CDCl_3$ ($4\cdot 3CDCl_3$). The crystal structure of the complex (Figure 1) shows the expected ligand bipyridine coordination mode with the Re(I) coordination sphere being composed of a "N_2C_3Cl" donor set. Selected bond lengths and angles are given in Table 2. The Re(I) ion lies in a distorted octahedral environment with three Re−C bonds of between 1.907(6) and 1.940(7) Å to the carbonyl ligands and two similar Re−N bonds of 2.180(4) and 2.192(4) Å to the bipyridine nitrogen donors. The Re−Cl bond length is 2.4731(14) Å. The 7-membered ring containing the O−P−O linkage that fuses the pyridyl rings of the bipyridyl ligand causes some distortion from the ideal ligand plane. Hence the mean planes of the coordinating pyridine rings are rotated by approximately 25° to one another, although the biphenyl moieties bound to the remaining two phosphorus atoms in the molecule have considerably larger interannular torsion angles of approximately 45°.

$[(L^4)Re(CO)_3Cl]\cdot 0.26H_2O$ ($7\cdot 0.26H_2O$). The crystal structure of the complex (Figure 2) shows essentially the

(38) (a) Allcock, H. R.; Sunderland, N. J.; Primrose, A. P.; Rheingold, A. L.; Guzei, I. A.; Parvez, M. *Chem. Mater.* **1999**, *11*, 2478–2485. (b) Cameron, T. S.; Borecka, B. *Phosphorus Sulfur* **1992**, *64*, 121–128. (c) Allcock, H. R.; Levin, M. L. *Acc. Chem. Res.* **1985**, *18*, 1324–1330. (d) Haddon, R. C.; Chichester-Hicks, S. V.; Mayo, S. L. *Inorg. Chem.* **1988**, *27*, 1911–1915. (e) Allcock, H. R. *Acc. Chem. Res.* **1978**, *11*, 81–87.

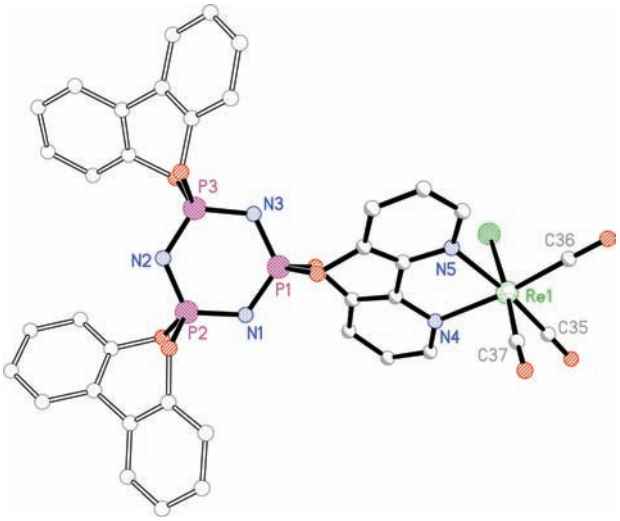

Figure 1. View of complex [(L [1])Re(CO)$_3$Cl] (**4**), with the hydrogen atoms removed for clarity.

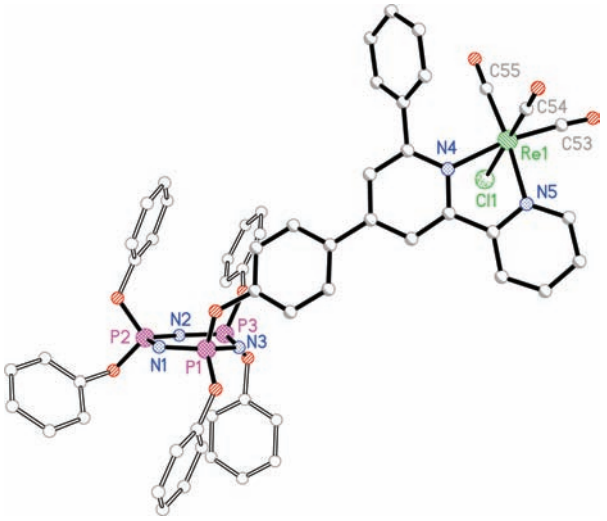

Figure 2. View of complex, [(L^4)Re(CO)$_3$Cl] (**7**), with the hydrogen atoms removed for clarity.

Table 2. Selected Bond Lengths (Å) and Angles (deg) for [(L^1)Re(CO)$_3$Cl] (**4**)

Re(1)−C(35)	1.925(6)	Re(1)−N(4)	2.192(4)
Re(1)−C(36)	1.907(6)	Re(1)−N(5)	2.180(4)
Re(1)−C(37)	1.940(7)	Re(1)−Cl(1)	2.4731(14)
P(1)−N(1)	1.560(5)	P(2)−N(2)	1.576(5)
P(1)−N(3)	1.567(5)	P(3)−N(2)	1.572(5)
P(2)−N(1)	1.586(5)	P(3)−N(3)	1.594(4)
C(35)−Re(1)−C(37)	87.8(3)	C(37)−Re(1)−N(5)	91.9(2)
C(36)−Re(1)−C(35)	87.2(3)	N(5)−Re(1)−N(4)	75.8(2)
C(36)−Re(1)−C(37)	88.9(3)	C(35)−Re(1)−Cl(1)	96.3(2)
C(35)−Re(1)−N(4)	98.3(2)	C(36)−Re(1)−Cl(1)	93.8(2)
C(36)−Re(1)−N(4)	173.5(2)	C(37)−Re(1)−Cl(1)	175.2(2)
C(37)−Re(1)−N(4)	94.8(2)	N(4)−Re(1)−Cl(1)	82.1(1)
C(35)−Re(1)−N(5)	174.0(2)	N(5)−Re(1)−Cl(1)	83.8(1)
C(36)−Re(1)−N(5)	98.8(2)		

Table 3. Selected Bond Lengths (Å) and Angles (deg) for [(L^4)Re(CO)$_3$Cl] (**7**)

Re(1)−C(53)	1.921(7)	Re(1)−N(4)	2.181(6)
Re(1)−C(54)	1.900(7)	Re(1)−N(5)	2.171(5)
Re(1)−C(55)	1.919(7)	Re(1)−Cl(1)	2.4932(16)
P(1)−N(1)	1.566(7)	P(2)−N(2)	1.585(7)
P(1)−N(3)	1.593(6)	P(3)−N(2)	1.571(7)
P(2)−N(1)	1.580(7)	P(3)−N(3)	1.579(6)
C(54)−Re(1)−C(53)	89.4(3)	C(55)−Re(1)−N(5)	173.1(2)
C(54)−Re(1)−C(55)	91.3(3)	N(5)−Re(1)−N(4)	74.7(2)
C(55)−Re(1)−C(53)	86.1(3)	C(53)−Re(1)−Cl(1)	91.7(2)
C(53)−Re(1)−N(4)	169.8(3)	C(54)−Re(1)−Cl(1)	178.3(2)
C(54)−Re(1)−N(4)	97.7(2)	C(55)−Re(1)−Cl(1)	90.0(2)
C(55)−Re(1)−N(4)	101.0(2)	N(4)−Re(1)−Cl(1)	81.0(1)
C(53)−Re(1)−N(5)	97.5(3)	N(5)−Re(1)−Cl(1)	83.9(1)
C(54)−Re(1)−N(5)	94.7(2)		

same coordination mode for the distorted octahedral Re(I) coordination sphere as **4**. Selected bond lengths and angles are given in Table 3. In this case the Re−C bonds range between 1.900(7) and 1.921(7) Å, and there are two similar Re−N bonds of 2.171(5) and 2.181(6) Å to the bipyridine nitrogen donors. The Re−Cl bond length is 2.4932(16) Å. The geometries about the coordinated/Re(I) centers in **4** and **7** are similar to those seen in [Re(phen)(CO)$_3$Cl] (phen = 1,10-phenanthroline);[39] however, the binding in **7** more closely resembles [Re(tpy)(CO)$_3$Cl] (tpy = 2,2′,2″-terpyridine) in which the tpy ligand acts in a bidentate manner.[40] The steric hindrance offered by the uncoordinated aromatic rings causes the bipyridine moiety to approach the metal at a slight angle. Hence, in [Re(tpy)(CO)$_3$Cl] and **7** the mean planes of coordinated bipyridine moieties lie at angles of 20 and 21°, respectively, to the mean coordination planes in which the nitrogen atoms bind. The torsion angle between the coordinated and the uncoordinated pyridine ring in [Re(tpy)(CO)$_3$Cl] is 130° and similar to the torsion angle of 129° between the coordinated pyridine ring and the 6-phenyl ring in **7**. This twisting still leaves short intramolecular contacts between the ipso-carbon atoms on the hypodentate rings and the nearest carbonyl ligands (3.082 and 3.067 Å respectively for [Re(tpy)(CO)$_3$Cl] and **7**). The oxygen atoms of these carbonyl ligands lie 3.254 and 3.204 Å from the centroid of the phenyl ring in **7** and pyridine ring in [Re(tpy)(CO)$_3$Cl] and could be considered as participating in intramolecular forms of π-carbonyl interactions that have been reported elsewhere.[41]

Vibrational Spectra. FT-IR spectra are dominated by aromatic ring deformations and are thus mostly similar for compounds of ligands with similar phosphazene-substitution (i.e., L^1 and L^2 are similar, as are L^3 and L^4). Carbonyl stretching frequencies, available for **4**−**7**, are however quite informative (Table 4). Most notably, the symmetric stretching mode of **4** at 2026 cm^{-1} appears red-shifted in **5**−**7** to 2021 cm^{-1}, which is consistent with decreased $\pi^*_L \rightarrow d\pi$ back-donation and suggests a slightly more electron-poor bipyridine unit.[42−44] Representative

(39) Haddad, S. F.; Marshall, J. A.; Crosby, G.; Twamley, B. *Acta Crystallogr., Sect. E* **2002**, *E58*, m559–m561.
(40) Civitello, E. R.; Dragovich, P. S.; Karpishin, T. B.; Novick, S. G.; Bierach, G.; O'Connell, J. F.; Westmoreland, T. D. *Inorg. Chem.* **1993**, *32*, 237–241.
(41) (a) Egli, M.; Sarkhel, S. *Acc. Chem. Res.* **2007**, *40*, 197–205. (b) Gambaro, A.; Ganis, P.; Manoli, F.; Polimeno, A.; Santi, S.; Venzo, A. *J. Organomet. Chem.* **1999**, *583*, 126–130.
(42) Worl, L. A.; Duesing, R.; Chen, P.; Della Ciana, L.; Meyer, T. J. *J. Chem. Soc., Dalton Trans.* **1991**, 849–858.
(43) Alsindi, W. Z.; Easun, T. L.; Sun, X. Z.; Ronayne Kate, L.; Towrie, M.; Herrera, J.-M.; George, M. W.; Ward, M. D. *Inorg. Chem.* **2007**, *46*, 3696–3704.
(44) Gamelin, D. R.; George, M. W.; Glyn, P.; Grevels, F.-W.; Johnson, F. P. A.; Klotzbuecher, W.; Morrison, S. L.; Russell, G.; Schaffner, K.; Turner, J. J. *Inorg. Chem.* **1994**, *33*, 3246–3250.

Table 4. Carbonyl Stretching Frequencies Found in the FT-IR Spectra of Compounds **4**−**7**[a]

ν(CO)/cm^{-1}				
4	**5**	**6**	**7**	symmetry
2026	2021	2021	2021	*a*′
1910	1916	1916	1921	*a*″
	1894	1896	1886	*a*′

[a] All measurements are in KBr. Symmetry assignments are from ref 44.

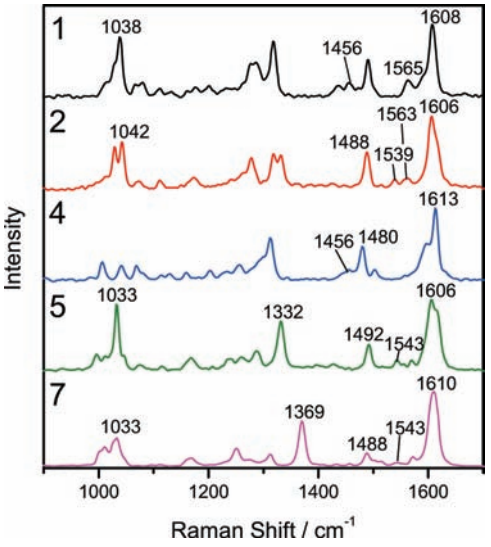

Figure 3. FT-Raman spectra of compounds **1**, **2**, **4**, **5**, and **7** acquired in KBr. Spectra of **3** and **6** are represented by those of **2** and **7**.

FT-Raman spectra are shown in Figure 3. The spectra of **3** and **6** share most of their main features with those of **2** and **7**, respectively, and are therefore omitted. As with FT-IR, spectra are dominated by aromatic ring deformations, most notably characteristic bpy and biphenyl stretches at about 1610 cm^{-1} as well as bpy breathing modes at about 1030 cm^{-1}. A number of minor peaks are highlighted, as they correspond to significant vibrational modes in resonance Raman (vide infra). It is important to quantify the quality of the calculated spectra, as this ensures that the calculations are producing an accurate picture of the electronic structure and allows other calculated data to be trusted. We do this by comparing the calculated vibrational spectra to the experimentally observed data; good correlation gives confidence in calculated quantities, such as structure, vibrational modes, and energetics.[30] The mean absolute deviations calculated lie between 8 and 10 cm^{-1} for Raman and IR spectra respectively, which is quite satisfactory considering a spectrometer resolution of 4 cm^{-1}.

Electronic Spectra. The electronic absorption spectra of **1**−**7** are shown in Figure 4, and the lowest-energy peaks are summarized in Table 5. The first eight calculated transitions with nonzero oscillator strengths can be found in the Supporting Information, Table S1. It should be noted that for the bimetallic compounds **3** and **6** the same low-energy transitions are calculated for each metal center, therefore essentially doubling each transition observed for compounds **2** and **5** respectively.

The absorption spectra of **2** and **3** are very similar to the spectrum of $[Ru(bpy)_3]^{2+}$,[45,46] where the band around 450 nm has been attributed to a (HOMO-2, HOMO-1) → (LUMO+1, LUMO+2) MLCT transition,[46] corresponding to the reduction of a single bipyridine ligand.[47] This is largely consistent with our assignment of the lowest-energy transition calculated at 414 nm (Supporting Information, Table S1). Although transitions with significant HOMO → LUMO character are calculated at lower energies, they show far lower oscillator strengths. They perhaps contribute to the red edge of the absorption band. In comparison, compound **1** shows a red-shift of the lowest-energy band to 468 nm. This is due to a lowering of the π^* molecular orbital energy with respect to the metal dπ orbital, indicating electron-deficiency caused by substitution with CTP.[42] Here the transition is calculated to originate from the HOMO-3 orbital, terminating on the HOMO and HOMO+2 orbitals. The decrease compared to **2** offsets the effect of the geometric constraints imposed by substitution of the bpy at two points, which increases the dihedral angle of the two pyridine rings from planarity to ∼8° according to DFT geometry calculations. The resulting decrease in conjugation is expected to slightly increase the π^* orbital energy and thus the energy of the MLCT transition; however, this is not observed. It should be noted that the increase is far greater for the equivalent rhenium compound (**4**), with a dihedral angle of ∼25°. From DFT calculations, the bpy 3,3′-H atoms of **1** are approximately 2.68 Å from the N atoms of the ancillary bpy ligands, which is shorter than the sum of their van der Waals radii. This suggests that perhaps intramolecular CH-π interactions are responsible for the decreased bipyridine dihedral angle of **1** compared to **4**, where ancillary bipyridine ligands are absent.

Compounds **5**−**7** show broad bands at about 392 nm, which are calculated by TD-DFT at about 410 nm as MLCT transitions originating predominantly in the HOMO-1 orbitals and terminating in the LUMO orbitals. A similar transition for $[Re(bpy)(CO)_3Cl]$ has previously been measured at 388 nm (in CH_2Cl_2)[48] and calculated at 403 nm (in MeCN, at the B3LYP/cc-pvdz level).[49] Molecular-orbital pictures (Figure 5) show that the relevant LUMOs are mostly localized on the bipyridine unit rather than the phenyl linker, indicating that conjugation with substituents plays only a small role in the lowest-energy excitation. The same applies to the 6-phenyl substituent of compound **7**. In the spectrum of **4** a similar band is found at a wavelength of 405 nm, mostly because of a HOMO-1 → LUMO transition calculated at 428 nm (Supporting Information, Table S1). As with **1**, a shift to higher wavelengths is due to an energy-decrease of the ligand π^* orbital. Compounds **3** and **6** each contain two metal-fluorophores, and for the UV−visible spectrum the extinction coefficient values for each are

(45) de Carvalho, I. M. M.; Moreira, I. d. S.; Gehlen, M. H. *Polyhedron* **2005**, *24*, 65–73.
(46) Gorelsky, S. I.; Lever, A. B. P. *J. Organomet. Chem.* **2001**, *635*, 187–196.
(47) Dallinger, R. F.; Woodruff, W. H. *J. Am. Chem. Soc.* **1979**, *101*, 4391–4393.
(48) Walters, K. A.; Kim, Y.-J.; Hupp, J. T. *Inorg. Chem.* **2002**, *41*, 2909–2919.
(49) Cannizzo, A.; Blanco-Rodriguez, A. M.; El Nahhas, A.; Sebera, J.; Zalis, S.; Vlcek, A., Jr.; Chergui, M. *J. Am. Chem. Soc.* **2008**, *130*, 8967–8974.

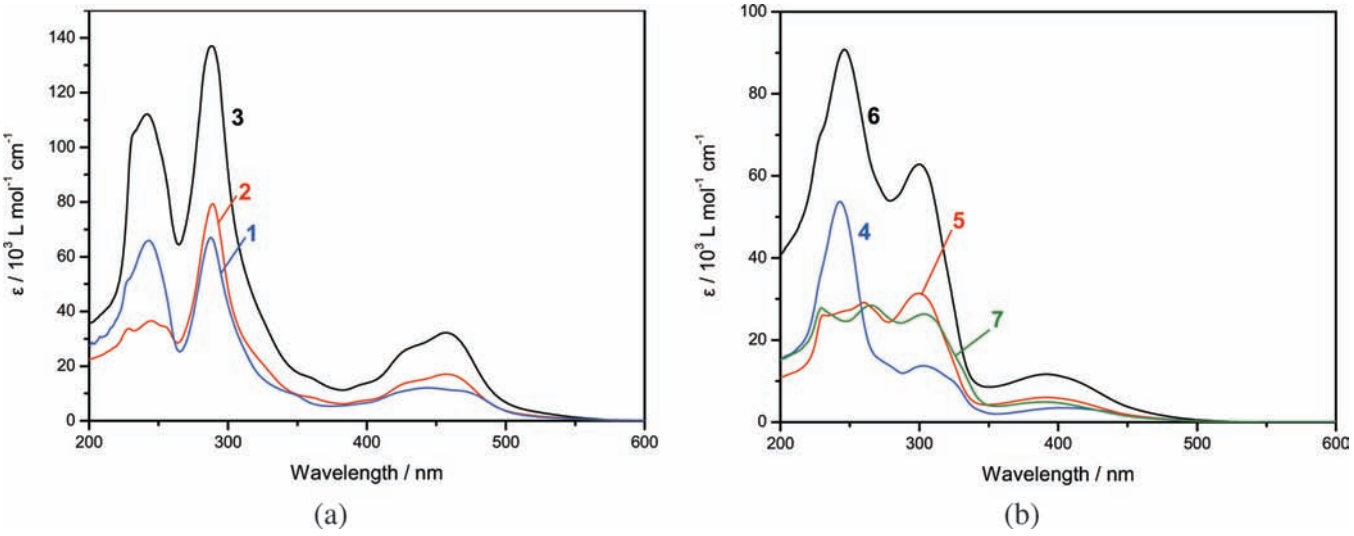

Figure 4. UV−visible spectra of (a) the ruthenium compounds and (b) the rhenium compounds. All spectra were acquired in dichloromethane.

Table 5. UV-Visible Absorption, Emission, and Lifetime Data[a]

compound	$\lambda_{abs}(\varepsilon)$/nm ($10^3$ M^{-1} cm^{-1})	λ_{em}/nm	τ/ns
1	468 (sh) (11)	647	380 ± 40
2	455 (17)	614	590 ± 60
3	454 (32)	613	670 ± 70
4	405 (3.5)	659	8 ± 1
5	392 (6.0)	629	47 ± 5
6	392 (12)	630	40 ± 10
7	392 (4.9)	634	27 ± 3
$[Ru(bpy)_3]^{2+}$[b]	452 (13)	597	680
$[Re(bpy)(CO)_3Cl]$[c]	388 (2.1)	598	39

[a] All measurements are at room temperature in dichloromethane. [b] From ref 52. [c] From ref 48.

essentially added, which is especially apparent at about 300 nm and higher wavelengths in comparison with **2** and **5**. This is strong evidence that there is no communication via CTP. The linear addition of absorbance breaks down around 240 nm, as this region corresponds to a $\pi \rightarrow \pi^*$ LC transition of the biphenyl moieties.[50,51] Therefore relatively little change in the UV−visible properties of compounds **1**−**7** is observed compared to $[Re(bpy)(CO)_3Cl]$ and $[Ru(bpy)_3]^{2+}$. Some electron-withdrawing properties are observed in the lowering of the π^*_L orbitals.

Generally the observed lifetimes and emission maxima are similar to those of the reference complexes $[Ru(bpy)_3]^{2+}$ [52] and [Re(bpy)(CO)3Cl].[48,53] For both complexes the emission is attributed to decay from a ^{3}MLCT state.[48,52,53] The fact that, for each sample, the emission spectra shows a single exponential (as a function of emission λ) is consistent with a single ^{3}MLCT emitting state for compounds **1**−**7**. The excited-state lifetimes are somewhat lower for compounds in which the bpy-CTP attachment is more intimate, compounds **1** and **4**, while their maximum emission wavelengths are increased. Making the assumption that the emission energy is comparable to the energy gap (i.e., $\Delta E \approx E_{em}$),[54] the change in lifetime is not inconsistent with the energy-gap law.[55,56] However, factors such as molecular rigidity or spin−orbit effects have to be considered as well to fully explain this. Shorter time-dynamics have been elucidated by Cannizzo et al. for $[Ru(bpy)_3]^{2+}$[57] and $[Re(bpy)(CO)_3Cl]$.[49] For $[Ru(bpy)_3]^{2+}$, population of a single ^{3}MLCT state is reported to occur on a 20 fs time scale through intersystem crossing (ISC) via the initially excited ^{1}MLCT state. For $[Re(bpy)(CO)_3Cl]$, ISC occurs to two ^{3}MLCT states in about 85−160 fs. Both states radiatively decay on a time scale of nanoseconds; however, since conversion from the higher to the lower ^{3}MLCT state occurs in less than 0.5 ps, phosphorescence is in practice only observed from the latter.

Resonance Raman (RR) Spectroscopy. RR shows selective enhancement of modes within active chromophores, where the excitation wavelength (λ_{ex}) determines which particular chromophore is being probed. This makes vibrational mode assignment by direct comparison to calculated spectra very difficult; however, it is possible via FT-Raman spectra, which show near-identical frequencies. The spectra of representative compounds acquired at 350.7 and 444.3 nm are shown in Figure 6a and Figure 6b and correspond to ligand-centered $\pi \rightarrow \pi^*$ and MLCT transitions respectively. Although spectra were also acquired at other wavelengths, these are omitted as they display band positions and intensities that are almost identical to the 444.3 nm spectrum. 444.3 nm was chosen as it gave a good signal-to-noise ratio, and it corresponds to transitions that are well into the MLCT regime for all compounds. Again, **3** and **6** are omitted as they show almost identical spectra to **2** and **5** respectively. The most significant vibrational modes are summarized in Table 6.

(50) Mulazzi, E.; Ripamonti, A.; Athouel, L.; Wery, J.; Lefrant, S. *Phys. Rev. B* **2002**, *65*, 085204/1–085204/9.
(51) Beenken, W. J. D.; Lischka, H. *J. Chem. Phys.* **2005**, *123*, 144311/1–144311/9.
(52) Durham, B.; Caspar, J. V.; Nagle, J. K.; Meyer, T. J. *J. Am. Chem. Soc.* **1982**, *104*, 4803–4810.
(53) Sato, S.; Sekine, A.; Ohashi, Y.; Ishitani, O.; Blanco-Rodriguez, A. M.; Vlcek, A. J.; Unno, T.; Koike, K. *Inorg. Chem.* **2007**, *46*, 3531–3540.
(54) Caspar, J. V.; Kober, E. M.; Sullivan, B. P.; Meyer, T. J. *J. Am. Chem. Soc.* **1982**, *104*, 630–632.
(55) Treadway, J. A.; Loeb, B.; Lopez, R.; Anderson, P. A.; Keene, F. R.; Meyer, T. J. *Inorg. Chem.* **1996**, *35*, 2242–2246.
(56) Damrauer, N. H.; Boussie, T. R.; Devenney, M.; McCusker, J. K. *J. Am. Chem. Soc.* **1997**, *119*, 8253–8268.
(57) Cannizzo, A.; van Mourik, F.; Gawelda, W.; Zgrablic, G.; Bressler, C.; Chergui, M. *Angew. Chem., Int. Ed.* **2006**, *45*, 3174–3176.

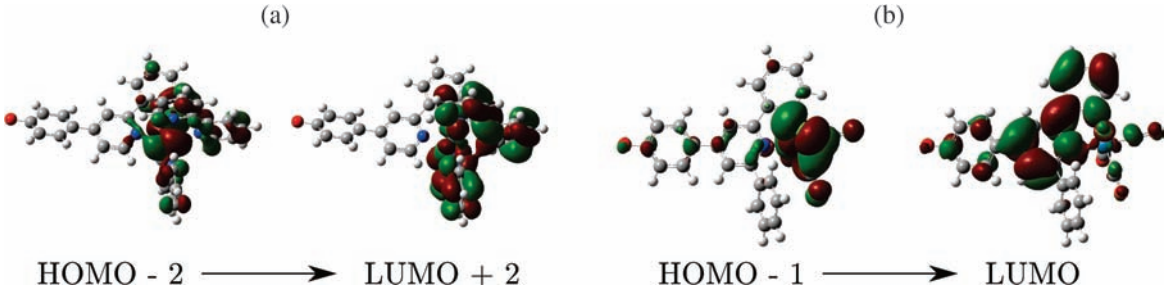

Figure 5. MO pictures of MLCT transitions of compounds **2** (a) and **7** (b) as calculated in a dichloromethane solvent field. The fluorophores on the ruthenium and rhenium compounds respectively show very similar MO pictures. The CTP units are omitted for clarity.

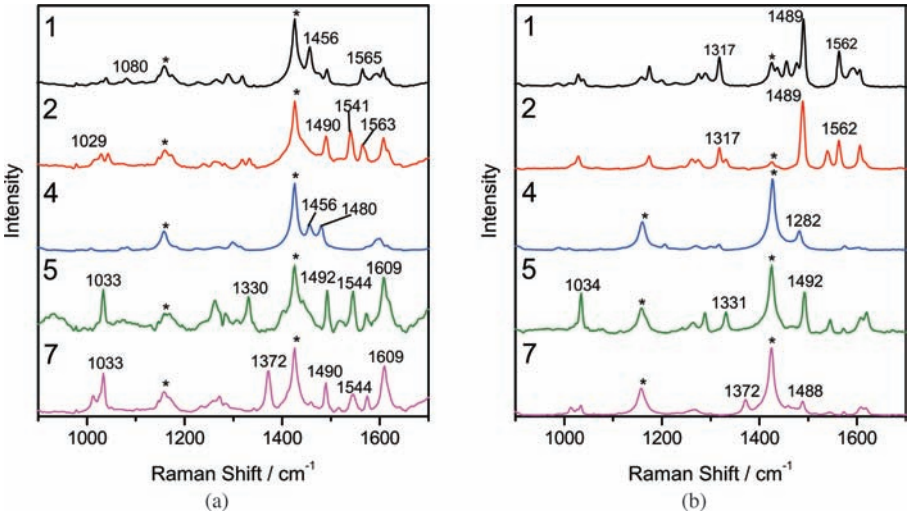

Figure 6. Resonance Raman (RR) spectra of compounds **1**, **2**, **4**, **5**, and **7** at excitation wavelengths (a) 350.7 nm and (b) 444.3 nm. All spectra were acquired in dichloromethane. The solvent peaks are marked by asterisks.

Table 6. Vibrational Modes Corresponding to Significant Peaks in the FT-Raman and Resonance Raman Spectra[a]

1556	1546	1540	1456	1372	1330
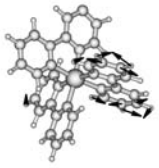	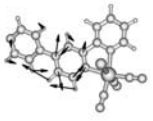		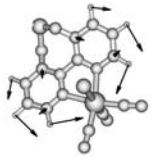		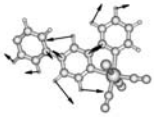
2, 3	**5, 6, 7**	**2, 3**	**1, 4**	**7**	**5, 6**

[a] Compounds displaying these or similar modes are listed.

At an excitation wavelength of 350.7 nm compound **1** shows resonance-enhancement of the modes at 1565 and 1080 cm^{-1}, and especially at 1456 cm^{-1}. While a vibration of the ancillary bpy ligands is responsible for the former, the latter two modes correspond to vibrations of the CTP-attached bpy ligand, which implies significant involvement in the transition of this moiety. In **2** (and thus **3**) resonance enhancement is seen in both CTP-attached and ancillary bpy ligands, for example, peaks at 1541 and 1563 cm^{-1} respectively. At 444.3 nm excitation, however, the features corresponding to ancillary bpy increase in relative intensity for compounds **1**−**3**. Especially marked in this respect are the peaks at about 1489 and 1317 cm^{-1}. This suggests that MLCT transitions involve predominantly the CTP-attached ligands while the more energetic $\pi \rightarrow \pi^*$ transitions occur on both CTP-attached and ancillary bipyridine ligands. The few peaks seen in the RR spectrum of **4** all correspond to bpy vibrations while, in comparison with the spectrum of **1** (Figure 6b), all vibrations due to ancillary bpy ligands are obviously absent. The mode at 1456 cm^{-1} is very similar to the one observed for **1**, and its absence at 444.3 nm supports the $\pi \rightarrow \pi^*$ assignment. The spectra of **5**−**7** are very similar to the RR spectrum of $[Re(bpy)(CO)_3Cl]$ measured by Smothers and Wrighton,[58] who assign the observed modes to vibrations of bpy. Comparison with DFT-calculated Raman modes confirms this (Table 6). Some differences exist between the spectra, however; compounds

(58) Smothers, W. K.; Wrighton, M. S. *J. Am. Chem. Soc.* **1983**, *105*, 1067–1069.

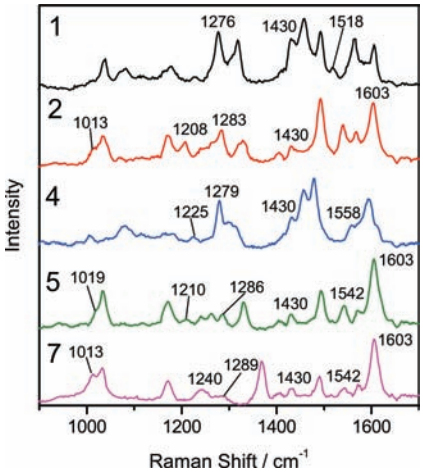

Figure 7. Transient resonance Raman spectra of some compounds acquired in dichloromethane at energies of 3.10 mJ/pulse. The solvent peaks have been subtracted for clarity.

5 and **6** show a bpy-deformation peak at 1330 cm^{-1}, while a similar mode is observed at 1372 cm^{-1} in the spectrum of **7** (Figure 6a). Accordingly, for **7** this mode involves the 6-substituted phenyl. Also observed is a totally symmetric carbonyl stretch at 2031 cm^{-1} for **4** and about 2026 cm^{-1} for **5**−**7**. This is further evidence for the presence of a MLCT state at wavelengths of 444.3 nm and higher as the relative intensity of these modes is stronger at these excitation-wavelengths.

Transient Resonance Raman (TR^2) Spectroscopy. TR^2 enables the examination of the excited-state structure in a similar fashion that RR is used for the ground-state. The leading edge of an intense laser pulse is used to generate molecules in the excited state, and the rest of the pulse then probes this state, provided the excited-state population is sufficiently high. Various pulse-energies (0.96 mJ/pulse, 1.84 mJ/pulse, and 3.10 mJ/pulse) were used to examine the variation in the amount of excited state generated. The photon to molecule ratio is about 30 for the highest pulse energy.[59] As with RR, the metal-bipyridyl unit is mostly responsible for the observed peaks. Therefore the TR^2 spectra of **3** and **6** are represented by those of **2** and **5**, respectively, in Figure 7. Identification of excited-state features is carried out by comparison to the ground state (λ_{ex} = 351 nm) resonance Raman spectra. A significant number of ground-state features are observed; however, also clearly visible are excited-state features corresponding to the radical anion of 2,2′- bipyridine ($bpy^{\cdot-}$).[47,58] Characteristic $bpy^{\cdot-}$ peaks are observed at about 1430, 1283, 1208, and 1013 cm^{-1} for **2** and **3**.[47] These values represent no obvious trend in terms of their differences from literature values for $[Ru(bpy)_3]^{2+}$; however, all are within 6 cm^{-1}. The peaks at about 1603 cm^{-1} occur with a higher relative intensity compared to the resonance Raman spectra. They appear similar to the peak at 1599 cm^{-1} in the excited-state resonance Raman spectrum of $[Ru(dpb)_3]^{2+}$ (dpb = 4,4′-diphenyl-2,2-bipyridine), measured by Damrauer et al.,[56] which suggests some phenyllinker involvement exists in the excited-state localization of the electron in compounds **2** and **3**. The modes observed for **1** are slightly red-shifted in comparison, indicating weaker binding within the bipyridine moiety in the triplet-state of this compound. This is good evidence for the localization of the excited-state electron on a single bipyridine moiety in compounds **1**−**3**. Compounds **4**−**7** generally show weaker excited-state features due to the lower excited-state population because of the decreased lifetimes; however, they are still visible. For example, **4** displays $bpy^{\cdot-}$ features at 1558, 1431 (observed in the solvent-subtracted spectrum) and 1279 cm^{-1}. Compounds **5** and **6** show excited-state features at about 1286, 1210 and as a shoulder at 1019 cm^{-1}, while similar peaks are observed at 1289, 1240, and 1013 cm^{-1} for **7**. They are again attributable to the bipyridine radical anion[58,60] and again deviations from literature-values of $[Re(bpy)(CO)_3Cl]$ exist, indicating involvement of the phenyl and therefore partial localization of the excited state on this moiety. As with the ruthenium compounds above, the peak at about 1603 cm^{-1} appears enhanced relative to the resonance Raman spectra, which supports this conclusion.

Conclusion

New cyclotriphosphazene ligands, L^1, L^2, L^3 and L^4, have been prepared from the reaction of sodium or cesium salts of the hydroxy species, $(HO)_2$bpy, HOPhbpy, and HOPhbpyPh with the appropriate cyclotriphosphazene precursors. The ruthenium- and rhenium-containing fluorophores attached to phosphazenes in the compounds **1**−**7** were obtained from the reactions of the free ligands with $[Ru(bpy)_2Cl_2]$ or $[Re(CO)_5Cl]$. All the compounds were characterized by elemental analyses, ^{31}P and ^1H NMR, and, in some cases, electrospray mass spectrometry. Two of the rhenium complexes, **4** and **7**, were also characterized by single crystal X-ray crystallography and shown to have the bipyridyl moiety coordinated giving a distorted octahedral "N_2C_3Cl" coordination sphere around the metal. Using resonance Raman, it was found that the transitions responsible for the bands at about 460 and 390 nm for the ruthenium and rhenium compounds, respectively, are metal to ligand charge-transfer in character, while the higher-energy bands are $\pi \rightarrow \pi^*$. This is in accordance with TD-DFT calculations, which were used to visualize the transition in terms of a HOMO/HOMO-1 → LUMO MLCT. Direct observation of the excited state $bpy^{\bullet-}$ radical anion with transient resonance Raman spectroscopy confirmed the localized nature of the excited states, similarly to $[Re(bpy)(CO)_3Cl]$ and $[Ru(bpy)_3]^{2+}$.

In conclusion, the study shows that the emissive properties of Ru(bpy) and Re(bpy) luminophores are not greatly perturbed when attached to CTP units if the covalent bonding is through a bpy linker substituent (such as a phenoxy group in L^2, L^3, and L^4). If the bpy luminophore is bound to the CTP unit directly through the 6,6′ positions (L^1), then the emissive properties are somewhat altered; however, they are not severely compromised. Generally, compounds **1**−**7** were shown to behave similarly to the corresponding metal bipyridyl-units without the CTP unit. This lack of interaction between fluorophore and chemically robust CTP unit has significance with respect to the potential applications of substituted cyclic phosphazenes in devices such as OLEDs. In principle, robust polymers may be formed from cyclic phosphazene that do

(59) Calculated by comparison of the number of photons in a single pulse (5.5×10^{15} photons at 350.7 nm) with the number of molecules in the sample. At a spot-size of approximately 300 μm and a penetration depth of 1 mm, the irradiated volume of sample is 2.83×10^{-7} L, which corresponds to 1.70×10^{14} molecules.

(60) Lewis, J. D.; Clark, I. P.; Moore, J. N. *J. Phys. Chem. A* **2007**, *111*, 50–58.

not affect the electronic properties of the metal complex. Effectively the phosphazene polymer could act as a highly chemically and thermally robust lattice holding electronic materials, such as luminophores and hole- and electron-transport units, within this matrix.

Acknowledgment. We thank Dr. K. Wagner for assistance with electrochemical measurements and gratefully acknowledge financial support from the Massey University Research Fund and RSNZ Marsden Funds (MAU208 and UOO0611). The support of the University of Otago, Foundation of Research Science and Technology, the Royal Society of New Zealand, and the MacDiarmid Institute for Advanced Materials and Nanotechnology is gratefully acknowledged.

Supporting Information Available: Crystallographic information for compounds **4**·3$CDCl_3$ and **7** in CIF format. TD-DFT transitions calculated for compounds **1**−**7**. This material is available free of charge via the Internet at http://pubs.acs.org.